88

REPORT NO.
UCB/SEMM-89/26

STRUCTURAL ENGINEERING,
MECHANICS AND MATERIALS

AN ELASTO-PLASTIC ANALYSIS OF REISSNER-MINDLIN PLATES

by

P. PAPADOPOULOS and R. L. TAYLOR

DECEMBER 1989

DEPARTMENT OF CIVIL ENGINEERING
UNIVERSITY OF CALIFORNIA AT BERKELEY
BERKELEY, CALIFORNIA

AN ELASTO-PLASTIC ANALYSIS OF REISSNER-MINDLIN PLATES

PANAYIOTIS PAPADOPOULOS[1] and *ROBERT L. TAYLOR*[2]

Department of Civil Engineering
University of California at Berkeley, Berkeley, CA, USA

ABSTRACT

A finite element analysis of elasto-plastic Reissner-Mindlin plates is presented. The discrete field equations are derived from a nonlinear version of the Hu-Washizu variational principle. Associative plasticity, including linear hardening, is employed by means of a generalized von Mises-type yield function. A predictor/corrector scheme is used to integrate the plastic constitutive rate equations. Numerical simulations are conducted for a series of test problems to illustrate performance of the formulation.

INTRODUCTION

Over the past two decades considerable effort has been directed towards the improvement of thick plate finite elements. Much of this work has been done within the context of linear elasticity. As a result, significant progress has been reported and new, efficient elements have emerged, see, e.g., [1,2,3]. These elements overcome the problem of transverse shear locking in the thin plate limit through the use of mixed interpolations and, at the same time, pass the patch test for pure bending.

This paper is devoted to inelastic analysis of plates, which include the effects of transverse shear deformation. The particular plate theory is commonly referred to as a Reissner-Mindlin theory and is based on results given in [4] and [5]. Here, the constitutive model is elasto-plastic and the presentation is given in resultant form, namely in terms of the stress resultants rather than the total stresses themselves. The choice of a resultant formulation is dictated by an attempt to save computational effort required in order to integrate local stresses through the plate thickness. The proposed model is based on an additive decomposition of strains and is viewed as a generalization of the plane stress associative model of von Mises. Indeed, the same model falls within the framework of classical elasto-plastic shell model proposed by Shapiro, [6], and recently extended to include hardening effects by Simo et al., [7].

The solution of the discrete inelastic problem is obtained incrementally using a full Newton method. Integration of the constitutive equations is performed by a predictor/corrector scheme, which features an initial elastic step, followed by elasto-plastic correction steps. This class of numerical algorithms (referred to as "return mapping algorithms" in the engineering literature) originates in the work of Wilkins, [8], and has been

---

[1] *Graduate Research Assistant*

[2] *Professor*

investigated in various contexts thereafter, see, e.g., [9,10,11].

The strain-driven nature of computational plasticity is becoming increasingly more appreciated. A continuum mechanics point of view is offered in [12]. Displacement control and continuation procedures (e.g., arc-length) are viewed as means of retaining convergence of iterative solutions by enforcing, in various manners, a contained load-displacement path. In this work, stress resultants are used in the algorithmic development, but it is implicitly understood that the energy conjugate strains are the primary variables of the problem.

The proposed algorithm is incorporated into the mixed triangular non-locking element presented in [13], and its performance is evaluated by a series of test problems.

1. REISSNER-MINDLIN PLATE BENDING THEORY

The plate model used here constitutes a simplification of the theories proposed by Reissner, [4], and Mindlin, [5]. It is based on the following assumptions:

(i) The domain Ω of the plate is of the form

$$\Omega = \left\{ (x,y,z) \in R^3 \;\middle|\; z \in [-\tfrac{1}{2}t, \tfrac{1}{2}t] \;,\; (x,y) \in A \subset R^2 \right\}$$

(ii) $$\sigma_{33} = 0$$

(iii) $$u = z\,\theta_y(x,y) \;,\; v = -z\,\theta_x(x,y) \;,\; w = w(x,y) \;,$$

where θ_x and θ_y are the rotations of transverse line elements about the x and y axes, respectively (e.g., see [14]). Assumption (iii) implies that straight normals to the reference surface, (z=0), remain straight, but do not necessarily remain normal to it after deformation takes place. Also the transverse displacement w does not depend upon the thickness. Assumption (ii) is obviously inconsistent with three-dimensional elasticity. However, the transverse normal stress may be neglected for plates where the thickness is small compared with the other dimensions. The constitutive equations are required to satisfy a plane stress condition augmented by transverse shear terms.

The assumed displacement field (iii) yields in-plane strains of the form

$$\epsilon_x = z\,\theta_{y,x} \;,\; \epsilon_y = -z\,\theta_{x,y} \;,\; \gamma_{xy} = z(\theta_{y,y} - \theta_{x,x}) \tag{1.1}$$

and transverse shear strains

$$\gamma_{xz} = w_{,x} + \theta_y \;,\; \gamma_{yz} = w_{,y} - \theta_x \tag{1.2}$$

The in-plane stresses, when integrated along the plate thickness yield stress resultants (moments) of the form :

$$M_x = \int_{-\frac{t}{2}}^{\frac{t}{2}} \sigma_x z dz \quad , \quad M_y = \int_{-\frac{t}{2}}^{\frac{t}{2}} \sigma_y z dz \quad , \quad M_{xy} = M_{yx} = \int_{-\frac{t}{2}}^{\frac{t}{2}} \sigma_{xy} z dz \tag{1.3}$$

In order to simplify the development, we introduce standard matrix notation and define

$$\mathbf{M} = \begin{bmatrix} M_x & M_y & M_{xy} \end{bmatrix}^T$$

and

$$\kappa(\theta) = \begin{bmatrix} \theta_{y,x} & -\theta_{x,y} & (\theta_{y,y} - \theta_{x,x}) \end{bmatrix}^T$$

Similarly, the out-of-plane stresses, when integrated along the thickness, give transverse shear forces

$$Q_x = \int_{-\frac{t}{2}}^{\frac{t}{2}} \sigma_{xz} dz \quad , \quad Q_y = \int_{-\frac{t}{2}}^{\frac{t}{2}} \sigma_{yz} dz \tag{1.4}$$

Again, in matrix notation we have

$$\mathbf{Q} = \begin{bmatrix} Q_x & Q_y \end{bmatrix}^T \quad , \quad \boldsymbol{\gamma} = \begin{bmatrix} (w_{,x} + \theta_y) & (w_{,y} - \theta_x) \end{bmatrix}^T$$

For further notational simplification, we establish the generalized force and strain vectors defined respectively as

$$\mathbf{S} = \begin{bmatrix} \mathbf{M} & \mathbf{Q} \end{bmatrix}^T \quad , \quad \mathbf{E} = \begin{bmatrix} \kappa & \boldsymbol{\gamma} \end{bmatrix}^T \tag{1.5}$$

In isotropic linear elasticity, the constitutive equations are written in terms of the above generalized vectors as

$$\begin{bmatrix} \mathbf{M} \\ \mathbf{Q} \end{bmatrix} = \begin{bmatrix} \mathbf{D}_b^e & \mathbf{0} \\ \mathbf{0} & \mathbf{D}_s^e \end{bmatrix} \begin{bmatrix} \kappa \\ \boldsymbol{\gamma} \end{bmatrix} ,$$

where

$$\mathbf{D}_b^e = \frac{Et^3}{12(1-\nu^2)} \begin{bmatrix} 1 & \nu & 0 \\ \nu & 1 & 0 \\ 0 & 0 & \frac{1-\nu}{2} \end{bmatrix}$$

and

$$\mathbf{D}_s^e = \kappa G t \mathbf{1}_2 = \bar{\alpha} \mathbf{1}_2$$

Note that κ is the correction parameter used to account for the assumption of constant transverse shear along the plate thickness. Also $\mathbf{1}_n$ denotes an $n \times n$ identity matrix. For further details, see [13].

2. RESULTANT STRESS ELASTO-PLASTICITY FORMULATION

In this section the underlying assumptions of the continuum elasto-plastic model are presented. Matrix notation is used extensively to facilitate algebraic manipulations.

2.1 Decomposition of strains

Within the realm of linearized kinematics, generalized strains are decomposed additively to elastic and inelastic (plastic) parts according to

$$\mathbf{E} = \mathbf{E}^e + \mathbf{E}^p \tag{2.1.1}$$

For the rationale and physical meaning of the above assumption, consult, e.g., [15].

Resultant stresses and elastic strains are related via the elastic moduli as

$$\mathbf{S} = \mathbf{D}^e\mathbf{E}^e = \mathbf{D}^e(\mathbf{E} - \mathbf{E}^p) \tag{2.1.2}$$

2.2 The yield criterion

As noted above, the Reissner-Mindlin plate theory considered here neglects the transverse normal stresses σ_{33}. This allows for a straightforward generalization of the von Mises plane stress yield function to include, in addition to the in-plane forces, the effect of transverse shear resultant forces, see Fig. (2.2.1). In stress space we define the dimensionless function

$$f(\mathbf{S}) = (M_x^2 + M_y^2 - M_xM_y + 3M_{xy}^2)\frac{1}{M_u^2} + (Q_x^2 + Q_y^2)\frac{1}{Q_u^2} \ , \tag{2.2.1}$$

where for homogeneous solid plates

$$M_u = \frac{t^2}{4}\sigma_y \quad , \quad Q_u = \frac{t}{\sqrt{3}}\sigma_y$$

and σ_y is the uniaxial yield stress.

Normalization of moments and shears in (2.2.1) is necessary for consistency. In matrix notation we have

$$f(\mathbf{S}) = \mathbf{S}^{\mathrm{T}}\mathbf{A}\mathbf{S} \ , \tag{2.2.2}$$

where

$$\mathbf{A} = \begin{bmatrix} \frac{1}{M_u^2}\mathbf{P} & \mathbf{0} \\ \mathbf{0} & \frac{1}{Q_u^2}\mathbf{I}_2 \end{bmatrix}$$

and

$$\mathbf{P} = \frac{1}{2}\begin{bmatrix} 2 & -1 & 0 \\ -1 & 2 & 0 \\ 0 & 0 & 6 \end{bmatrix}$$

Taking into account (2.1.2), we may rewrite (2.2.2) in strain space as

$$f(\mathbf{S}(\mathbf{E}^e)) = g(\mathbf{E}^e) = \mathbf{E}^{e\,T}\mathbf{B}\mathbf{E}^e \quad , \tag{2.2.3}$$

with

$$\mathbf{B} = \mathbf{D}^e\mathbf{A}\mathbf{D}^e$$

Linear hardening is accommodated by admitting the existence of an internal variable ξ, which constitutes a measure of the plastic deformation. We define ξ at time τ as

$$\xi = \int_0^\tau [\frac{2}{3}(\Theta\dot{\mathbf{E}}^p):(\Theta\dot{\mathbf{E}}^p)]^{1/2} d\tau' \quad , \tag{2.2.4}$$

where

$$\Theta = \begin{bmatrix} \frac{1}{2}\mathbf{1}_3 & \mathbf{0} \\ \mathbf{0} & \mathbf{1}_2 \end{bmatrix}$$

Consequently, we may write the yield criterion in strain space as

$$\Phi(\mathbf{E}^e,\xi) = g(\mathbf{E}^e) - \left(\frac{\sigma_y + H\xi}{\sigma_y}\right)^2 \quad , \tag{2.2.5}$$

with H being an isotropic linear hardening parameter.

2.3 Flow rule and consistency condition

We consider an associative flow rule which is expressed as

$$\dot{\mathbf{E}}^p = \dot{\gamma}\mathbf{D}^{e\,-1}\frac{\partial\Phi}{\partial\mathbf{E}^e} \tag{2.3.1}$$

Taking into account (2.2.3) and (2.2.4), we obtain

$$\dot{\mathbf{E}}^p = \dot{\gamma}\mathbf{G} \quad , \tag{2.3.2}$$

where

$$\mathbf{G} = 2\mathbf{A}\mathbf{S} = 2\mathbf{A}\mathbf{D}^e\mathbf{E}^e$$

and $\dot{\gamma}$ is a parameter to be determined by enforcing the plastic consistency condition. Note that, despite the fact that the plastic flow is specified in rate form, the constitutive law is rate-independent.

The consistency condition dictates that, during plastic loading, stresses (strains) remain on the yield surface in stress (strain) space. Enforcing this condition in strain space and noting from (2.2.4) and (2.3.2) that

$$\dot{\xi} = [\frac{2}{3}(\Theta\dot{\mathbf{E}}^p):(\Theta\dot{\mathbf{E}}^p)]^{1/2}$$

we have by means of (2.2.5)

$$\dot{\Phi}(\mathbf{E}^e,\xi) = 0$$

or using (2.2.3)

$$(\mathbf{D}^e\mathbf{G}):\dot{\mathbf{E}}^e - 2\sqrt{(\frac{2}{3})}\dot{\gamma}H\frac{(\sigma_y + H\xi)}{\sigma_y^2}|\Theta\mathbf{G}| = 0 \ ,$$

where

$$|\Theta\mathbf{G}| = \left[(\Theta\mathbf{G}):(\Theta\mathbf{G})\right]^{\frac{1}{2}}$$

Consequently,

$$\dot{\gamma} = \sqrt{(\frac{3}{2})}\frac{\sigma_y^2}{2(\sigma_y + H\xi)H}\frac{(\mathbf{D}^e\mathbf{G}):\dot{\mathbf{E}}^e}{|\Theta\mathbf{G}|} \qquad (2.3.3)$$

2.4 Variational formulation

In order to allow mixed finite element approximations, we introduce a variational (weak) form of the momentum balance equations for the elasto-plastic problem. The formulation is based on the total potential energy for bending and on the Hu-Washizu three-field principle, [16], for the transverse shear. The inelastic version of the functional is made possible by defining the stored (elastic) energy W as

$$W = W(\theta,\gamma) = \frac{1}{2}\kappa^{e\,T}\mathbf{D}_b^e\kappa^e + \frac{1}{2}\gamma^{e\,T}\mathbf{D}_s^e\gamma^e$$

where

$$\kappa^e = \kappa(\theta) - \kappa^p \ , \ \gamma^e = \gamma - \gamma^p$$

and in matrix notation

$$W = W(\theta,\gamma) = \frac{1}{2}\mathbf{E}^{e\,T}\mathbf{D}^e\mathbf{E}^e$$

Accordingly, the functional form of the variational equations is

$$\Pi_1(\theta,w,\mathbf{Q},\gamma) = \int_A W dA - \int_A \mathbf{Q}^T(\gamma - \nabla w - \mathbf{e}\theta)dA - \int_A wq dA + \Pi_{EXT} \ , \qquad (2.4.1)$$

where the alternating tensor $\mathbf{e}$ is defined as

$$\mathbf{e} = \begin{bmatrix} 0 & 1 \\ -1 & 0 \end{bmatrix}$$

and Π_{EXT} describes the effect of boundary and other loads.

It should be noted that in order to retain a strain-based formulation, it is ultimately necessary that the transverse stress resultants $\mathbf{Q}$ in (2.4.1) be dependent on strain quantities.

2.5 The elasto-plastic problem - minimization statement

In view of the formulation developed in the above subsections, we obtain the quadratic minimization problem which may be stated as;

$$\text{minimize } \Pi_1$$

subject to the Kuhn-Tucker loading/unloading unilateral constraints

$$\Phi \leq 0 \text{ and } \dot{\gamma} \geq 0 \text{ with } \dot{\gamma}\Phi = 0 .$$

3. DISCRETE SOLUTION OF THE ELASTO-PLASTIC PROBLEM

The continuum elasto-plastic problem is tackled numerically on an incremental basis by discretizing the (implicit) time involved in the rate equations (2.3.2) and computing iteratively the resulting generalized stress-strain response function.

The discrete algorithmic problem can be stated as follows;

Given: previous state of strains and total strain increment

$$\left\{ \mathbf{E}_n , \mathbf{E}_n^p , \xi_n \right\} \quad , \quad \left\{ \Delta \mathbf{E} \right\} ,$$

respectively, at time $\tau = \tau_n$.

Compute: the state of strains

$$\left\{ \mathbf{E}_{n+1} , \mathbf{E}_{n+1}^p , \xi_{n+1} \right\}$$

at the current time $\tau = \tau_{n+1}$.

3.1 Flow equations and consistency condition

The flow equations (2.3.2) and the internal variable evolution equation (2.2.4) are integrated by the unconditionably stable backwards Cauchy-Euler method yielding

$$\mathbf{E}_{n+1}^p = \mathbf{E}_n^p + \lambda_{n+1} \mathbf{G}_{n+1} \quad , \tag{3.1.1}$$

$$\xi_{n+1} = \xi_n + \lambda_{n+1} \sqrt{\left(\frac{2}{3}\right)} \left| \Theta \mathbf{G}_{n+1} \right| \quad , \tag{3.1.2}$$

where

$$\lambda_{n+1} = \gamma_{n+1} - \gamma_n$$

In addition, the discrete consistency condition

$$\Phi(\mathbf{E}_{n+1}^e , \xi_{n+1}) = 0 \tag{3.1.3}$$

has to be fulfilled.

Equations (3.1.1) and (3.1.3) are implicit and generally have to be solved iteratively. For this reason, they are rewritten as

$$\mathbf{R} = \mathbf{E}^p_n + \lambda_{n+1}\mathbf{G}_{n+1} - \mathbf{E}^p_{n+1} = \mathbf{0} \ ,$$

$$r = -\Phi(\mathbf{E}_{n+1} - \mathbf{E}^p_{n+1} \ , \xi_{n+1}) = 0$$

and a Newton scheme is employed to solve them. Specifically, given a state (i) of the local Newton iteration (at every Gauss point in each finite element), we solve

$$\mathbf{R}^{(i+1)}_{n+1} = \mathbf{R}^{(i)}_{n+1} + \frac{\partial \mathbf{R}}{\partial \mathbf{E}^p_{n+1}}\Delta\mathbf{E}^{p\,(i)}_{n+1} + \frac{\partial \mathbf{R}}{\partial \lambda_{n+1}}\Delta\lambda^{(i)}_{n+1} = \mathbf{0} \tag{3.1.4}$$

$$r^{(i+1)}_{n+1} = r^{(i)}_{n+1} + \frac{\partial r}{\partial \mathbf{E}^p_{n+1}}\Delta\mathbf{E}^{p\,(i)}_{n+1} + \frac{\partial r}{\partial \lambda_{n+1}}\Delta\lambda^{(i)}_{n+1} = 0 \tag{3.1.5}$$

Taking into account (3.1.1-3) along with (2.3.1), (2.3.2) and (2.2.5), the above equations are written in matrix form as

$$\begin{bmatrix} \mathbf{R}^{(i)}_{n+1} \\ r^{(i)}_{n+1} \end{bmatrix} = \begin{bmatrix} \mathbf{1}_5 + \lambda^{(i)}_{n+1} 2\mathbf{A}\mathbf{D}^e & -\mathbf{G}^{(i)}_{n+1} \\ -\mathbf{G}^{T\,(i)}_{n+1}\mathbf{D}^e & \Omega \end{bmatrix} \begin{bmatrix} \Delta\mathbf{E}^{p\,(i)}_{n+1} \\ \Delta\lambda^{(i)}_{n+1} \end{bmatrix} \ , \tag{3.1.6}$$

where

$$\Omega = -2\sqrt{(\frac{2}{3})}\frac{H}{\sigma_y}\left\{1 + \frac{H}{\sigma_y}(\xi_n + \frac{2}{3}\lambda^{(i)}_{n+1}|\mathbf{G}^{(i)}_{n+1}|)\right\}|\mathbf{G}^{(i)}_{n+1}|$$

The initial guess for λ_{n+1} and $\mathbf{E}^p_{n+1}$ is based on the assumption that the imposed increment of strains is purely elastic (elastic predictor), namely that

$$\lambda^{(0)}_{n+1} = 0 \quad , \quad \mathbf{E}^{p\,(0)}_{n+1} = \mathbf{E}^p_n$$

The subsequent steps account for the plastic deformation that the applied increment of strains $\Delta\mathbf{E}$ produces (plastic correctors), according to

$$\mathbf{E}^{p\,(i+1)}_{n+1} = \mathbf{E}^{p\,(i)}_{n+1} + \Delta\mathbf{E}^{p\,(i)}_{n+1}$$

$$\lambda^{(i+1)}_{n+1} = \lambda^{(i)}_{n+1} + \Delta\lambda^{(i)}_{n+1}$$

Convergence of the above iterative scheme is guaranteed, since the yield surface described by (2.2.5) is convex.

3.2 Elasto-plastic tangent modulus

The importance of using consistent (algorithmic) elasto-plastic tangent moduli, as opposed to continuum moduli is demonstrated in [9].

Total differentiation of (2.1.2) gives the differential form

$$d\mathbf{S}_{n+1} = \mathbf{D}^e(d\mathbf{E}_{n+1} - d\mathbf{E}^p_{n+1}) \tag{3.2.1}$$

Similarly, the discrete flow equation (3.1.1), when differentiated, yields

$$d\mathbf{E}^p_{n+1} = \lambda_{n+1} 2\mathbf{A} d\mathbf{S}_{n+1} + \mathbf{G}_{n+1} d\lambda_{n+1} \ , \tag{3.2.2}$$

while for the hardening variable ξ

$$d\xi_{n+1} = \sqrt{(\frac{2}{3})}|\Theta \mathbf{G}_{n+1}|\, d\lambda_{n+1} \tag{3.2.3}$$

Substituting (3.2.3) into the algorithmic consistency condition

$$\mathbf{G}_{n+1}{:}d\mathbf{S}_{n+1} - 2H\frac{\sigma_y + H\xi_{n+1}}{\sigma_y^2}d\xi_{n+1} = 0 \ ,$$

we may solve for $d\lambda_{n+1}$ and substitute along with (3.2.2) into (3.2.1) to find

$$\left\{\mathbf{D}^{e\ -1} + \lambda_{n+1}2\mathbf{A} + \frac{\mathbf{G}_{n+1}\mathbf{G}_{n+1}^T}{M}\right\}d\mathbf{S}_{n+1} = d\mathbf{E}_{n+1} \ ,$$

where

$$M = -2H\sqrt{(\frac{2}{3})}\frac{\sigma_y + H\xi_{n+1}}{\sigma_y^2}|\Theta \mathbf{G}_{n+1}|$$

Therefore, in matrix notation

$$\mathbf{D}_{n+1}^{ep\ -1}d\mathbf{S}_{n+1} = d\mathbf{E}_{n+1} \tag{3.2.4}$$

It is important that $\mathbf{D}_{n+1}^{ep\ -1}$ in (3.2.4) be inverted explicitly, because otherwise perfect plasticity (H=0) cannot be handled.

Explicit inversion is easily performed for

$$\mathbf{H}_{n+1}^{-1} = \mathbf{D}^{e\ -1} + \lambda_{n+1}2\mathbf{A} \ ,$$

so then using the Sherman-Morrison formula for rank-one updates we finally have

$$\mathbf{D}_{n+1}^{ep} = \mathbf{H}_{n+1} - \frac{\mathbf{H}_{n+1}\mathbf{G}_{n+1}\mathbf{G}_{n+1}^T\mathbf{H}_{n+1}}{\mathbf{G}_{n+1}^T\mathbf{H}_{n+1}\mathbf{G}_{n+1} + M} \tag{3.2.5}$$

The elasto-plastic tangent moduli evaluated in (3.2.5) is of the general form

$$\mathbf{D}^{ep} = \begin{bmatrix} \mathbf{D}_b^{ep} & \mathbf{D}_{bs}^{ep} \\ \mathbf{D}_{bs}^{ep\ T} & \mathbf{D}_s^{ep} \end{bmatrix} \ , \tag{3.2.6}$$

where clearly the off-diagonal terms (absent in the elastic case), indicate coupling between bending and transverse shear, due to the contained nature of the plastic deformation.

Nonlinearity of the stress-strain relation is evident from (3.2.5) and implies that the momentum balance equations stemming from the minimization of the discrete counterpart of (2.4.1) must be solved by a global (at the assemblage level) Newton scheme.

3.3 Discrete solution - summary

Implementation of the discrete solution of the elasto-plastic plate problem is summarized in Box 1;

BOX 1. Return Mapping algorithm

1. Given $\mathbf{E}_n$, $\mathbf{E}^p_n$, ξ_n and $\Delta\mathbf{E}$

   Compute elastic predictor

   $$\mathbf{E}^{p\,(0)}_{n+1} = \mathbf{E}^p_n$$

   $$\xi^{(0)}_{n+1} = \xi_n$$

2. For every Gauss point compute

   $$\Phi(\mathbf{E}^{e\,(0)}_{n+1}\ ,\ \xi_n)$$

2a. If $\Phi \leq 0$ step elastic (use elastic stiffness)

   $$\mathbf{E}^p_{n+1} = \mathbf{E}^p_n$$

   EXIT

2b. If $\Phi \geq 0$ step plastic

3. Solve system (3.1.4-5) iteratively with initial guess

   $$\mathbf{E}^{p\,(0)}_{n+1} = \mathbf{E}^p_n$$

   $$\lambda^{(0)}_{n+1} = 0$$

   to get λ_{n+1} , $\mathbf{E}^p_{n+1}$

4. Compute the elasto-plastic tangent stiffness (3.2.6)

5. Assemble global stiffness $\mathbf{K}_{n+1}$ and residual $\mathbf{R}_{n+1}$

5a. If $\mathbf{R}_{n+1} \approx \mathbf{0}$ (within tolerance)

   CONVERGENCE ATTAINED

   Compute stresses, displacement, etc.

   EXIT

5.b Else solve

   $$\mathbf{R}_{n+1} = \mathbf{K}_{n+1}\Delta\mathbf{u}_{n+1}$$

   for $\Delta\mathbf{u}_{n+1}$

   Set $\mathbf{u}_{n+1} \leftarrow \mathbf{u}_{n+1} + \Delta\mathbf{u}_{n+1}$

   Go to step 1

3.4 Application of the algorithm

The proposed algorithm is applied to a conforming mixed triangular plate element called DRM3, [13], which is based on (2.4.1). In the DRM3 element the following type of interpolation is implemented :

$$w = \mathbf{N}_w \hat{\mathbf{w}} + \mathbf{N}_{w\theta}\hat{\boldsymbol{\theta}} \quad , \quad \boldsymbol{\theta} = \mathbf{N}_\theta \hat{\boldsymbol{\theta}} \quad ,$$

$$\boldsymbol{\gamma} = \mathbf{N}_\gamma \hat{\boldsymbol{\gamma}} \quad , \quad \mathbf{Q} = \sum_{k=1}^{3} \delta(x - x_k) \mathbf{t}_k \overline{Q}_t^k \quad ,$$

where δ is the Dirac function, $\mathbf{t}_k$ is the tangent to the element side and $\overline{Q}_t^k$ is the tangential shear stress at the midpoint k of the element side. In particular, $\boldsymbol{\theta}$ is assumed to vary according to

$$\boldsymbol{\theta} = \sum_{i=1}^{3} L_i \hat{\boldsymbol{\theta}}_i = \sum_{i=1}^{3} 4 L_i L_j \mathbf{n}_k \Delta\theta \hat{\boldsymbol{\theta}}_k \quad ,$$

where j = mod(i,3) + 1 , k = mod(j,3) + 1, L_i are the standard area coordinates, {17], and $\mathbf{n}_k$ is the normal to the edge k.

Furthermore, w is interpolated according to

$$w = \sum_{i=1}^{3} L_i \hat{w}_i = \sum_{i=1}^{3} 4 L_i L_j (\alpha_k L_i + \beta_k L_j) \quad ,$$

where the parameters α_l and β_l, l=1,2,3 are to be determined by requiring the tangential shear strain to be *constant along each edge of the triangle*. Additional details are provided in [13].

The functional (2.4.1) is extremized with respect to Q producing the constraint equation

$$\int_A \delta\mathbf{Q}(\boldsymbol{\gamma} - \nabla w - \mathbf{e}\boldsymbol{\theta}) dA = 0 \quad ,$$

which leads to

$$\hat{\boldsymbol{\gamma}} = \mathbf{Q}_\theta \hat{\boldsymbol{\theta}} + \mathbf{Q}_w \hat{\mathbf{w}}$$

Introducing the strain-displacement matrix $\mathbf{B}_b$ as

$$\mathbf{B}_b = \begin{bmatrix} 0 & -\dfrac{\partial \mathbf{N}_\theta}{\partial y} & -\dfrac{\partial \mathbf{N}_\theta}{\partial x} \\ \dfrac{\partial \mathbf{N}_\theta}{\partial x} & 0 & \dfrac{\partial \mathbf{N}_\theta}{\partial y} \end{bmatrix}^T \quad ,$$

we evaluate curvatures and shear strains respectively as

$$\boldsymbol{\kappa} = \mathbf{B}_b \hat{\boldsymbol{\theta}}$$

and similarly

$$\boldsymbol{\gamma} = \mathbf{B}_{s\theta} \hat{\boldsymbol{\theta}} + \mathbf{B}_{sw} \hat{w}$$

Finally, minimization of (2.4.1) with respect to θ and w and use of the elasto-plastic tangent modulus (3.3.6) leads, for each element, to a matrix equation of the form

$$\begin{bmatrix} \mathbf{K}_{\theta\theta} & \mathbf{K}_{\theta w} \\ \mathbf{K}_{w\theta} & \mathbf{K}_{ww} \end{bmatrix} \begin{Bmatrix} \Delta\theta \\ \Delta w \end{Bmatrix} = \begin{bmatrix} \mathbf{R}_\theta \\ \mathbf{R}_w \end{bmatrix} ,$$

where

$$\mathbf{K}_{\theta\theta} = \int_A \{ \mathbf{B}_b{}^T \mathbf{D}_b^{ep} \mathbf{B}_b + \mathbf{B}_b{}^T \mathbf{D}_{bs}^{ep} \mathbf{B}_{s\theta} +$$

$$\mathbf{B}_{s\theta}{}^T \mathbf{D}_{bs}^{ep\ T} \mathbf{B}_b + \mathbf{B}_{s\theta}{}^T \mathbf{D}_s^{ep} \mathbf{B}_{s\theta} \} dA ,$$

$$\mathbf{K}_{\theta w} = \mathbf{K}_{w\theta}^T = \int_A \{ \mathbf{B}_b{}^T \mathbf{D}_{bs}^{ep} \mathbf{B}_{s\theta} + \mathbf{B}_{s\theta}{}^T \mathbf{D}_s^{ep} \mathbf{B}_{sw} \} dA ,$$

$$\mathbf{K}_{ww} = \int_A \mathbf{B}_{sw}^T \mathbf{D}_s^{ep} \mathbf{B}_{sw} \, dA$$

and $\mathbf{R}_\theta$, $\mathbf{R}_w$ are the residual forces.

4. NUMERICAL EXAMPLES

A series of numerical simulations were conducted to evaluate the performance of the model and the numerical algorithm. All results are compared to existing analytical solutions (either exact or in the form of upper and/or lower bounds) for thin plates. Computations have been performed within the environment of the Finite Element Analysis Program (FEAP), (e.g. see Chap. 15 of [17]).

Unless otherwise stated, the following values of parameters have been used for the test problems:

$$\text{Young's modulus} \quad E = 10.92 ,$$

$$\text{Poisson's ratio} \quad \nu = 0.3 ,$$

$$\text{Uniaxial yield stress} \quad \sigma_y = 1000 .$$

Convergence of the global Newton scheme is monitored through the energy norm defined for iteration (i) by

$$E^{(i)} = \int_A \mathbf{S}_{n+1}^{(i)} \mathbf{E}_{n+1}^{(i)} dA$$

and the tolerance for convergence in the above norm is set to 10^{-16}. A three-point Gauss quadrature has been used for the numerical integration of the element arrays.

4.1 Simply-supported point-loaded square plate

A simply-supported square plate has been modeled with two different meshes (MS1 and MS2) and has been subjected to a point load P acting at its center. Due to symmetry, only a quarter of the plate is actually analyzed, see Fig. (4.1). Hard simply supported boundary conditions have been imposed (see, e.g., [2] or [13]).

The plate thickness is t = 0.1 and the side length is a = 10.

For the case of perfect plasticity (H=0) the numerical collapse load is compared to an upper bound for the thin plate given in [18], see Fig. (4.1.1). In addition, analyses have been performed using mesh MS1 for H=0.05 and 0.10, see Fig. (4.1.2). The evolution of plastic deformation for the perfectly plastic case is illustrated in Fig. (4.1.3).

4.2 Simply-supported uniformly loaded square plate

The same plate as in 4.1 has been analyzed for a uniform transverse load q and H=0. The approximate critical loading obtained is compared to upper and lower bound estimates for the thin plate as reported in [15], see Fig. (4.2.1). Again, plots of the mesh indicating the plastic regions for various steps are provided, Fig. (4.2.2).

4.3 Clamped uniformly loaded square plate

The uniform mesh MS1 along with the selectively refined mesh MS3, Fig. (4.1), are used to discretize the clamped plate with geometric properties as in 4.1 . An upper bound for the thin plate is derived in [15] and is shown in Fig. (4.3.1) along with the solution obtained by the finite element analysis for H = 0. Fig. (4.3.2) shows various steps of plastification obtained during the numerical simulation.

4.4 Simply-supported uniformly loaded circular plate

Uniform meshes MC1 and MC2, Fig. (4.4), are used to model a simply-supported circular plate under uniform load q. Due to symmetry only one quarter of the plate is discretized. The thickness of the plate is t=0.1 and the radius R=5. The estimated ultimate load is compared to the numerical exact solution for the Kirchhoff plate reported in [15]. Since the plate to thickness ratio is small, good agreement is expected and, in fact, obtained, see Fig. (4.4.1). The evolution of plastic deformation is illustrated in Fig. (4.4.2).

In order to assess the effect of transverse shear deformation in the plastic process, a parametric analysis is performed for plates with constant M_u and the previously used radius (therefore the same Kirchhoff limit load), but with different thicknesses and uniaxial yield stresses. Mesh MC5 is used throughout the analysis. Fig. (4.4.3) confirms that the effect of shear becomes significant as the thickness to radius ratio increases.

4.5 Clamped uniformly loaded circular plate

Fine discretization is required for the clamped circular plate under uniform load q in order to produce results featuring satisfactory agreement with the numerical exact solution for the ultimate load in the thin plate limit, see [15]. The geometric data for the test problem are as in 4.4 . Selectively refined meshes MC3 and MC4 appear in Fig. (4.4). Refinement is necessary both along the clamped edge and towards the center of the plate. Load-

displacement and plastic evolution diagrams are presented in Fig. (4.5.1) and (4.5.2) respectively.

4.6 Simply-supported uniformly loaded triangular plate

A plate having the shape of an equilateral triangle with side length a=12 and thickness t=0.1 is subjected to a uniform load q. Soft simply supported boundary conditions are employed (see [13]). Numerical simulations were conducted for a half of the plate and uniform meshes MT1 and MT2 are shown in Fig. (4.6). The load-displacement diagram is given in Fig. (4.6.1), while the history of plastic deformation that leads to collapse is indicated in Fig. (4.6.2). The computed ultimate load is below the upper bound calculated in [18] for the Kirchhoff plate.

CONCLUSION

The theoretical and numerical aspects of an elasto-plastic analysis of thick plates are addressed. Both the constitutive equations and the weakly enforced momentum balance equations are written in resultant form. The numerical solution consists of an implicit local integration scheme for the constitutive equations in the plastic regime and a global iterative procedure that eliminates the residual of the momentum balance equations. The overall performance of the numerical solution is excellent in terms of both stability for large time steps and accuracy in simulating various test problems.

Acknowledgment

The help of Prof. J. Lubliner is greatly appreciated.

REFERENCES

[1] T.J.R. Hughes and T.E. Tezduyar, "Finite elements based upon Mindlin plate theory with particular reference to the four node bilinear isoparametric element", *J. Appl. Mech.*, 46, 587-596, (1981).

[2] O.C. Zienkiewicz, R.L. Taylor, P. Papadopoulos and E. Onate, "Plate bending elements with discrete constraints: New triangular elements", UCB/SEMM Rep. 89/09, Dept. Civ. Engr., UCB, (1989).

[3] E.N. Dvorkin and K.J. Bathe, "A continuum mechanics based four node shell element for general non-linear analysis", *Eng. Comp.*, 1, 77-88, (1984).

[4] E. Reissner, "The effect of transverse shear deformation on the bending of elastic plates", *J. Appl. Mech.*, 12, 69-76, (1945).

[5] R.D. Mindlin, "Influence of rotatory and shear on flexural motions of isotropic, elastic plates", *J. Appl. Mech.*, 18, 31-38, (1951).

[6] G.S. Shapiro, "On yield surfaces for ideal plastic shells", in **Problems of Continuum Mechanics**, p.414-418, SIAM, Philadelphia, (1961).

[7] J.C. Simo and J.G. Kennedy, "On a stress resultant geometrically exact shell model. Part VI. Nonlinear plasticity: Formulation and integration algorithms", to appear in *Comp. Meth. App. Mech. Engr.*, (1990).

[8] M.L. Wilkins, "Calculation of plastic flow", in **Methods of Computational Physics** 3, Academic Press, New York, (1964).

[9] J.C. Simo and R.L. Taylor, "Consistent tangent operators for rate-independent elastoplasticity", *Comp. Meth. Appl. Mech. Engr.*, 48, 101-118, (1985).

[10] M. Ortiz and E.P. Popov, "Accuracy and stability of integration algorithms for elastoplastic constitutive relations", *Int. J. Num. Meth. Engr.*, 21, 1561-1576, (1985).

[11] J.C. Simo and R.L. Taylor, "A return mapping algorithm for plane stress elastoplasticity", *Int. J. Num. Meth. Engr.*, 22, 649-670, (1986).

[12] P.M. Naghdi and J.A. Trapp, "The significance of formulating plasticity theory with reference to loading surfaces in strain space", *Int. J. Engr. Sc.*, 13, 785-797, (1975).

[13] P. Papadopoulos and R.L. Taylor, "A triangular element based on Reissner-Mindlin plate theory", to appear in *Int. J. Num. Meth. Engr.*, (1990).

[14] T.J.R. Hughes, **The Finite Element Method**, Englewood Cliffs, N.J.: Prentice-Hall, (1987).

[15] J. Lubliner, **Plasticity Theory**, Macmillan, New York, to appear (1990).

[16] K. Washizu, **Variational Methods in Elasticity and Plasticity**, Oxford: Pergammon Press, (1982).

[17] O.C. Zienkiewicz and R.L. Taylor, **The Finite Element Method**, 4th ed., Vol. 1, McGraw-Hill, London, (1989).

[18] W. Johnson and P.B. Mellor, **Engineering Plasticity**, Van Nostrand Reinhold, London, (1973).

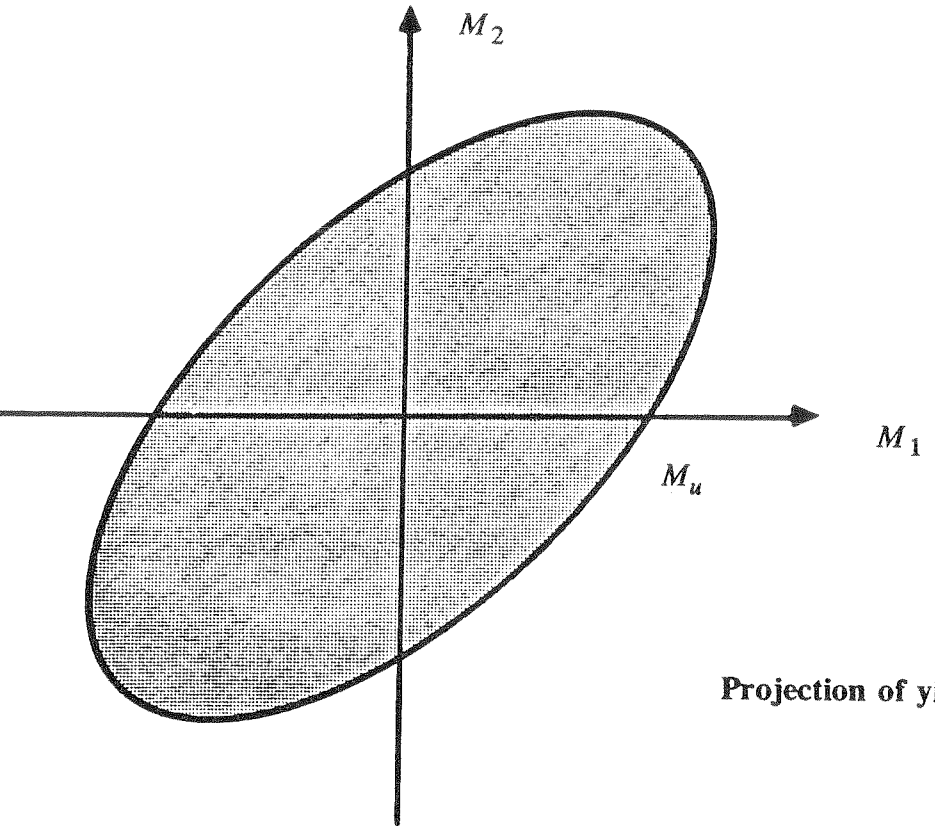

Projection of yield function on principal moments

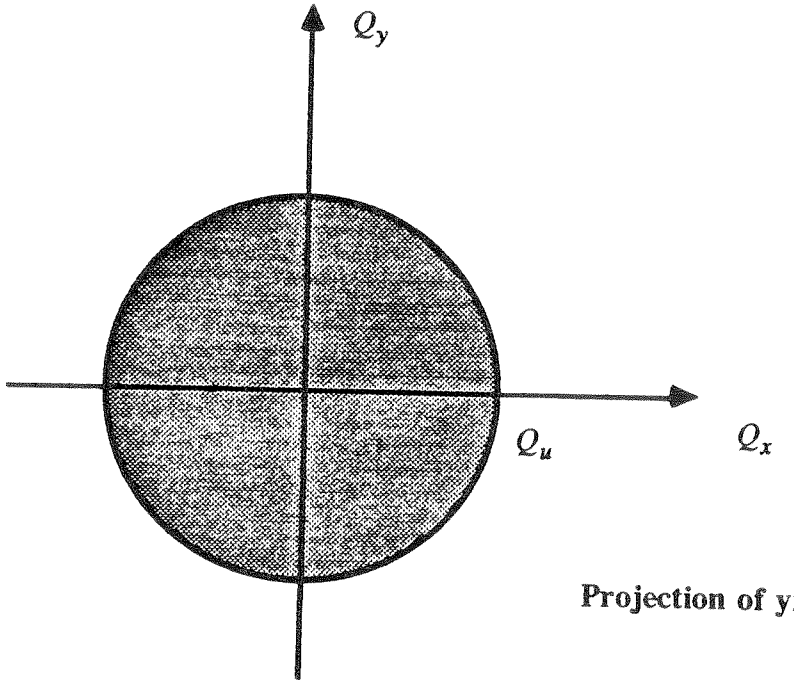

Projection of yield function on tranverse shear resultants

Fig. 2.2.1 Yield function in stress space

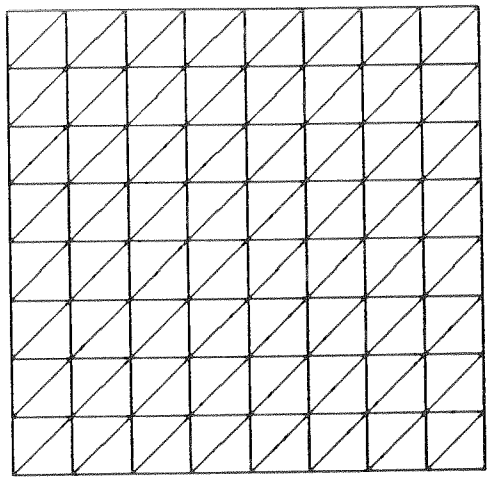

C
L

C
L

MS1

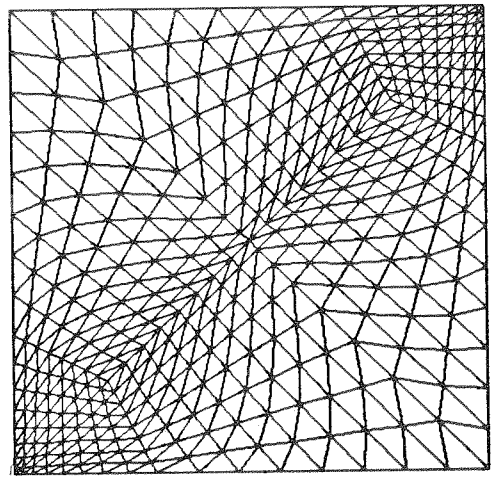

C
L

C
L

MS2

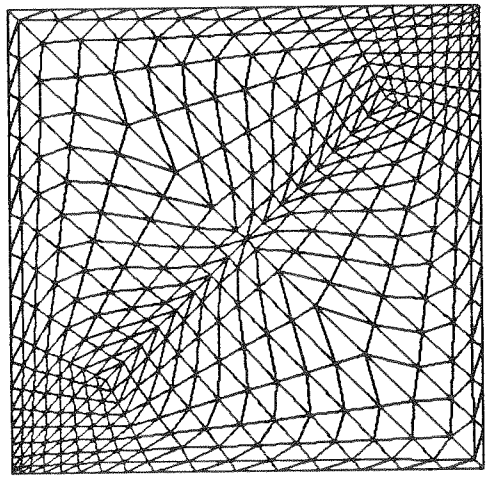

C
L

C
L

MS3

Fig. 4.1 Square meshes

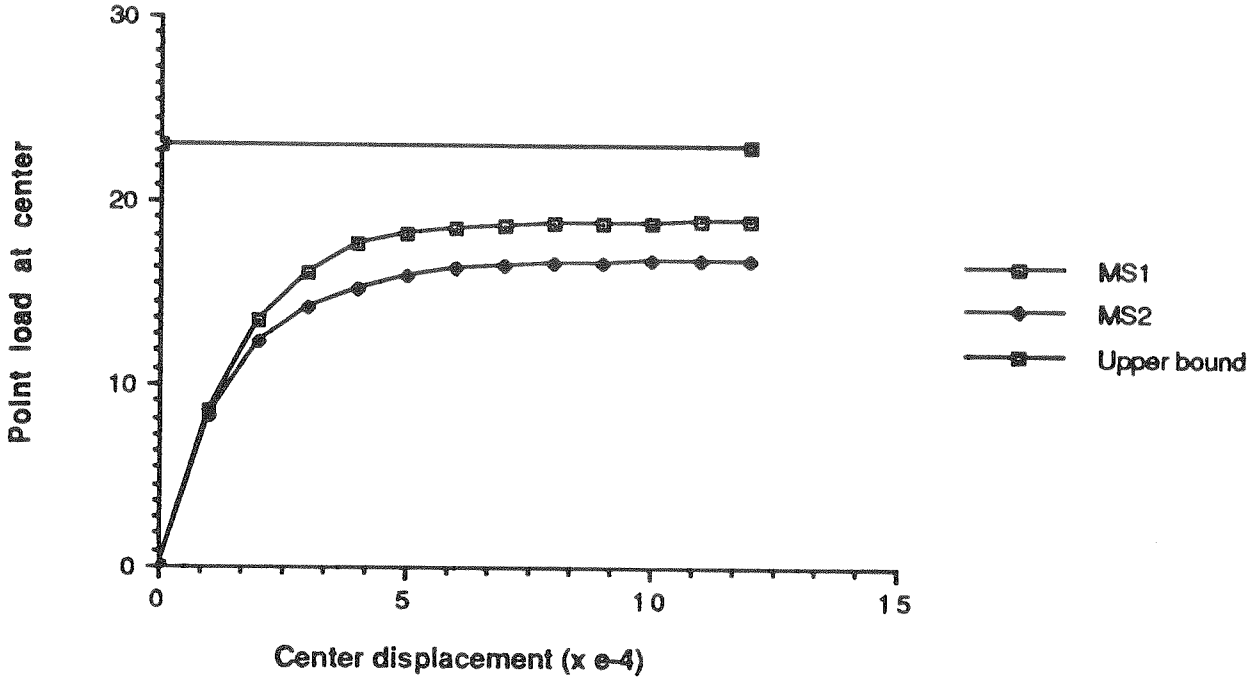

Fig. 4.1.1 Simply-supported point loaded square plate; load-displacement diagram

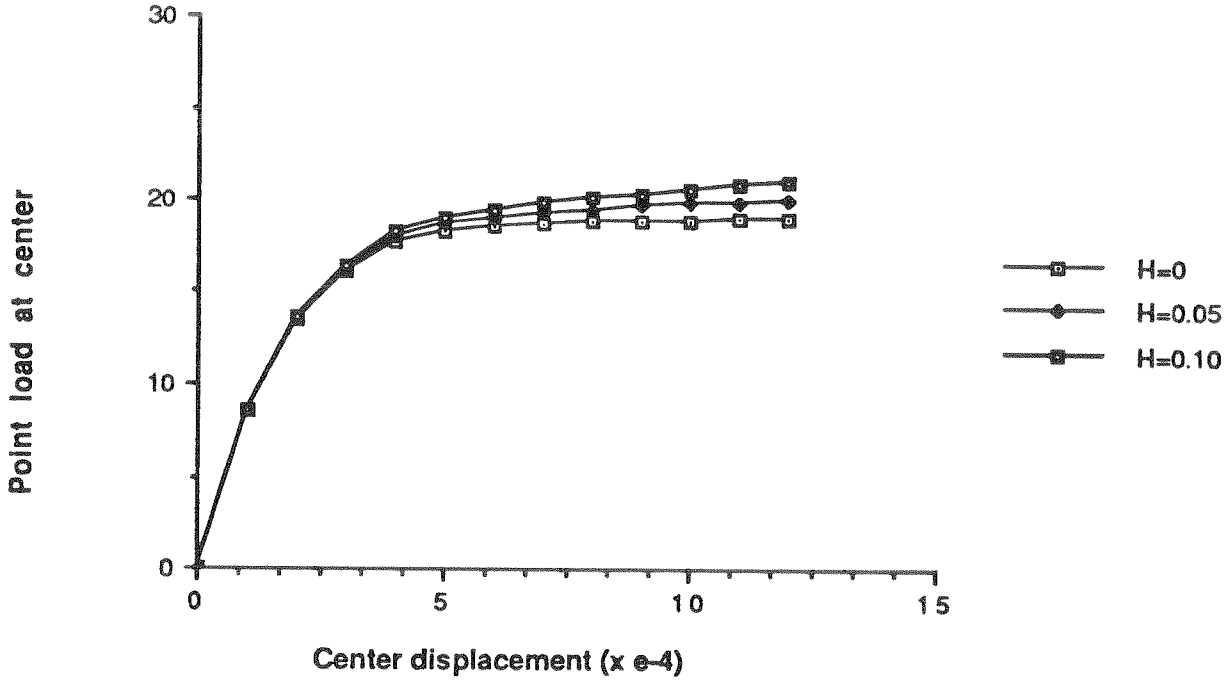

Fig. 4.1.2 Simply-supported point loaded square plate; load-displacement diagram for various values of H

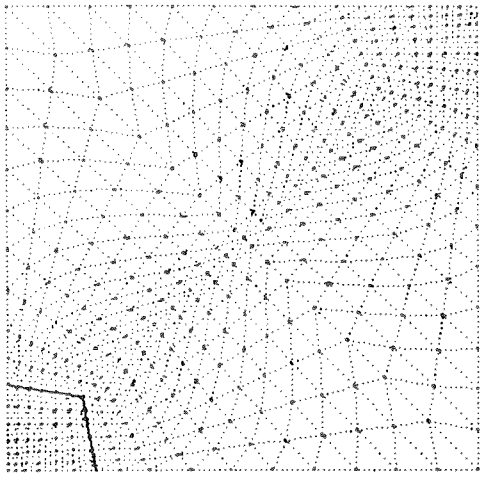

P= 12.308

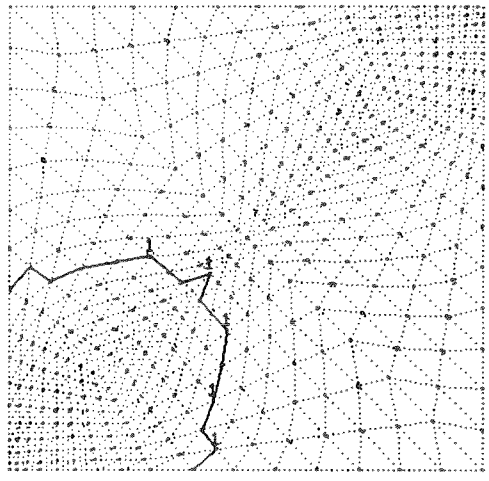

P= 15.944

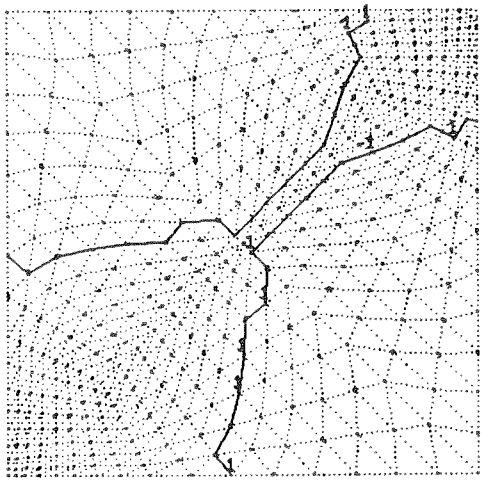

P= 16.364

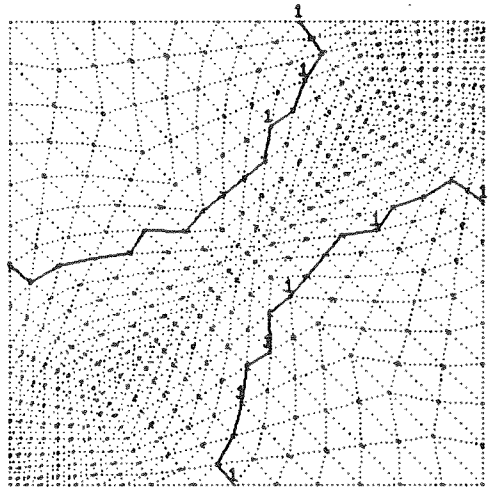

P= 16.544

Fig. 4.1.3 Simply-supported point loaded square plate; evolution of plastic deformation (mesh MS2)

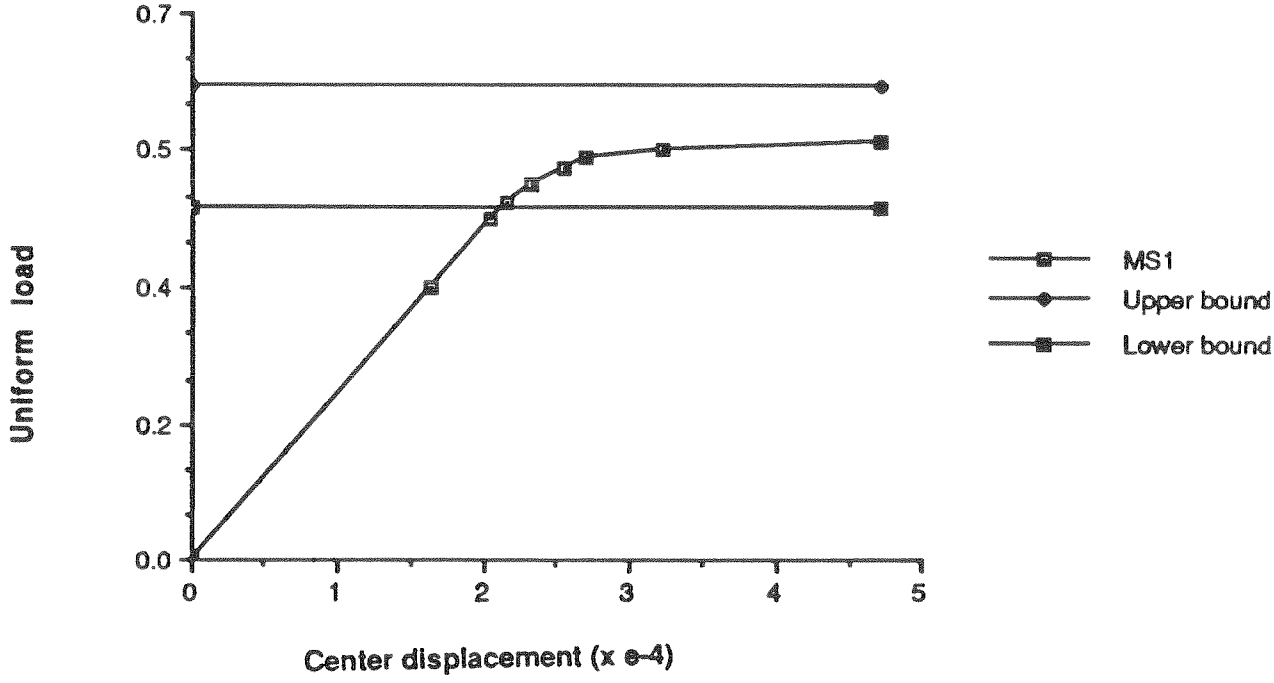

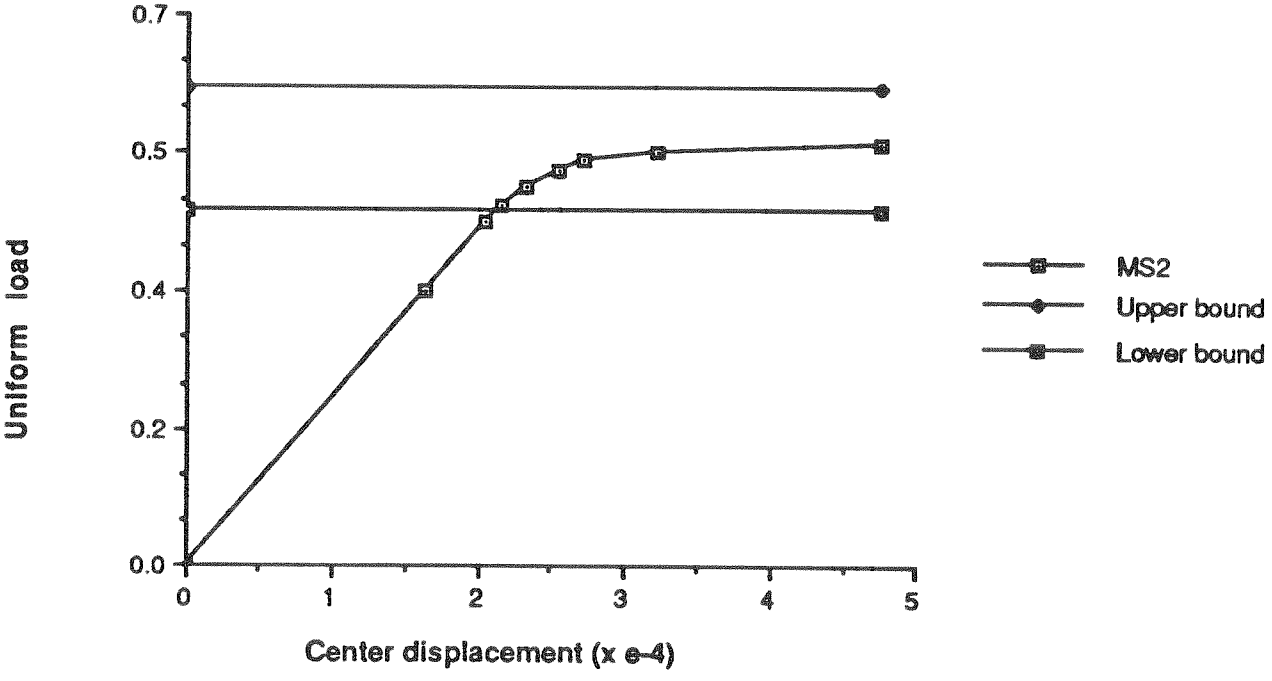

Fig. 4.2.1 Simply-supported uniformly loaded square plate; load-displacement diagrams

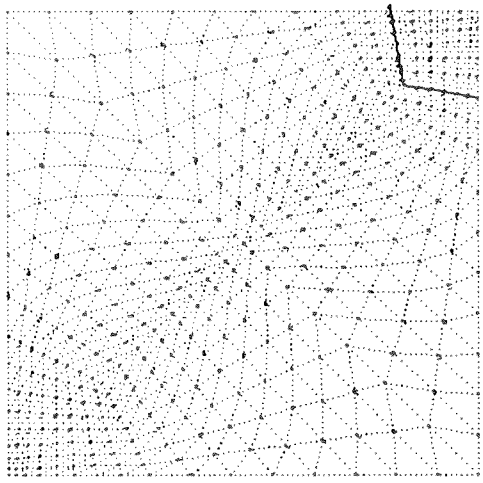

q=0.50

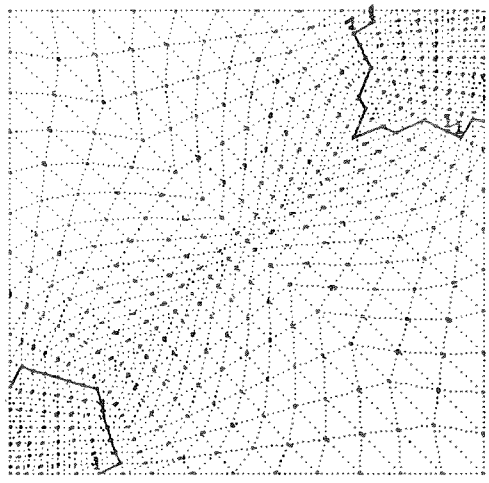

q=0.55

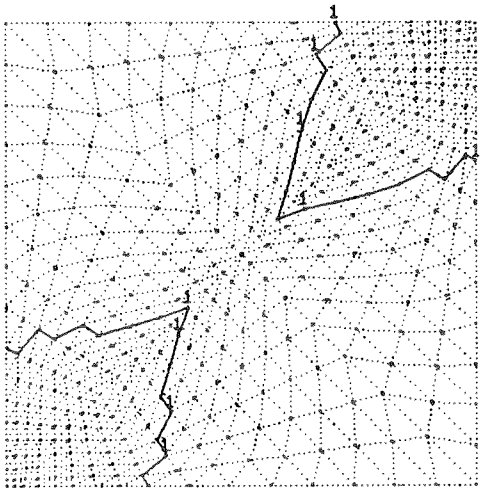

q=0.5875

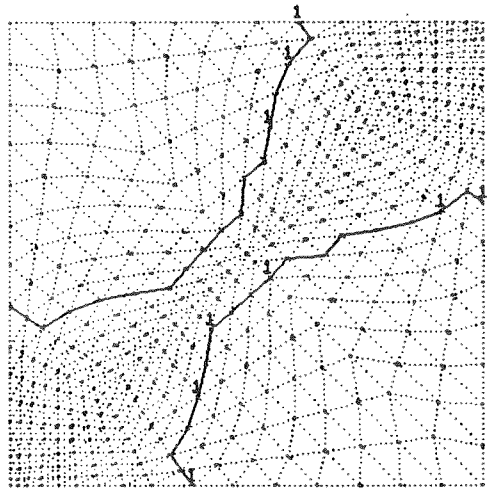

q=0.60

Fig. 4.2.2 Simply-supported uniformly loaded square plate; evolution of plastic deformation (mesh MS2)

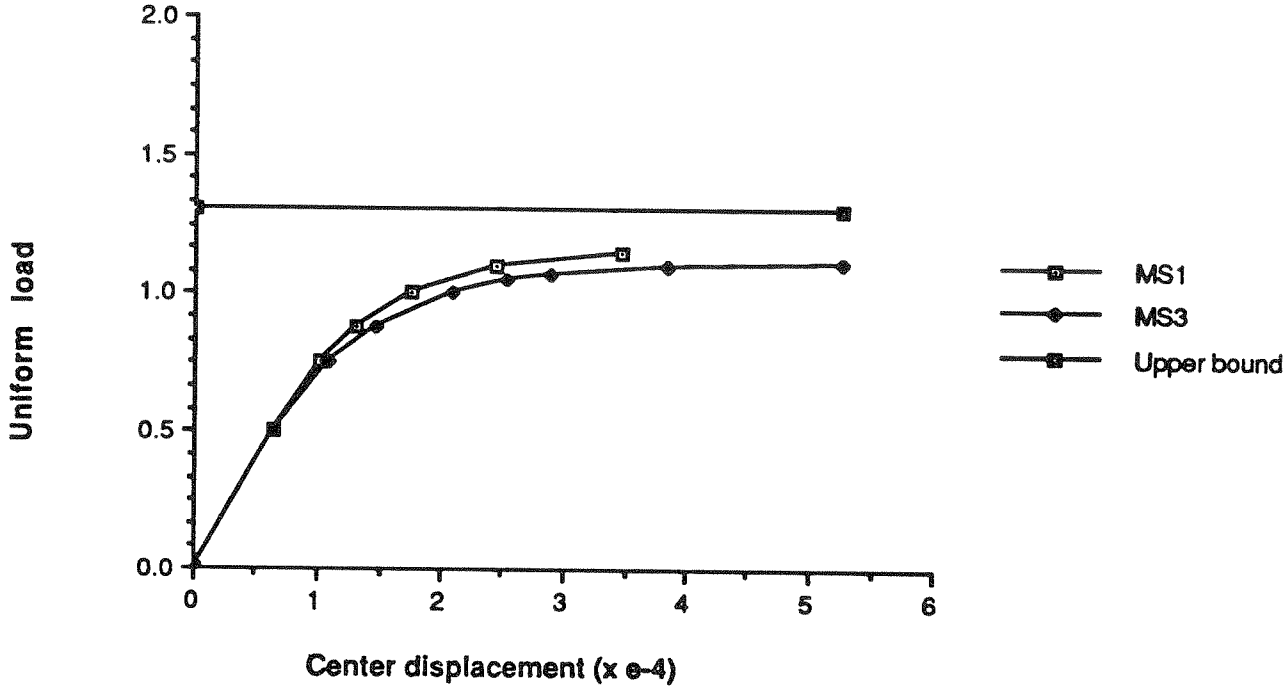

Fig. 4.3.1 Clamped uniformly loaded square plate; load-displacement diagram

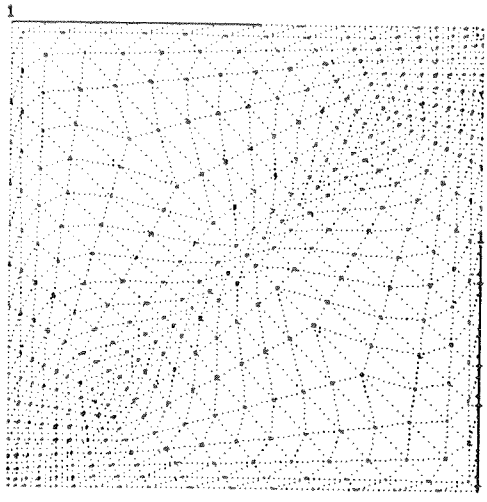

q=0.75

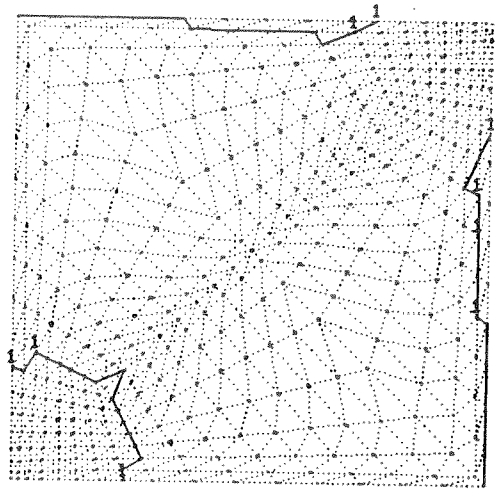

q=1.0

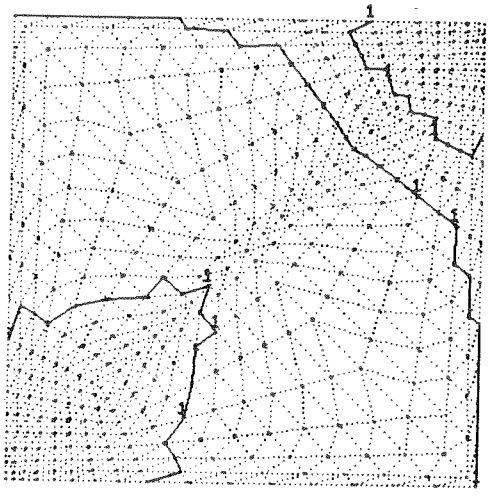

q=1.075

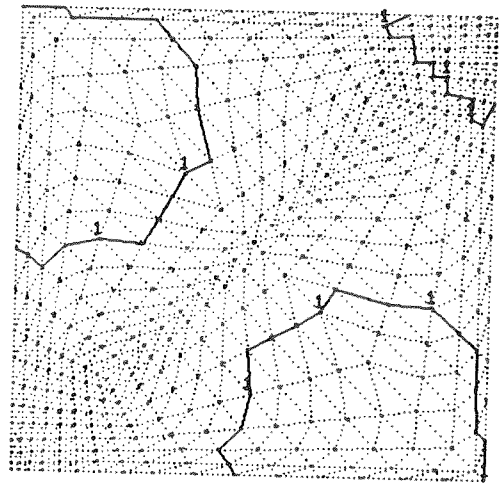

q=1.1125

Fig. 4.3.2 Clamped uniformly loaded square plate;
evolution of plastic deformation (mesh MS3)

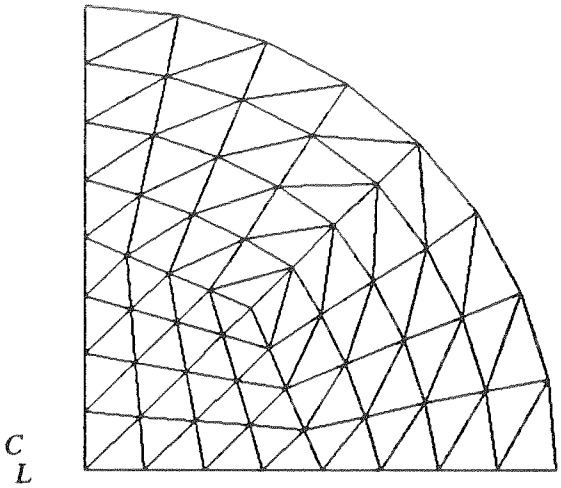

C
L

MC1

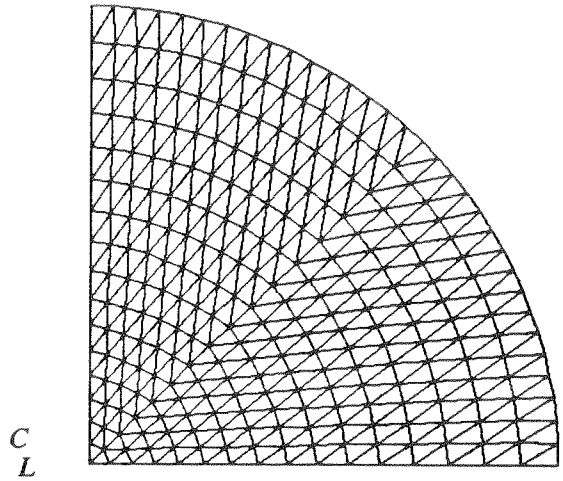

C
L

MC2

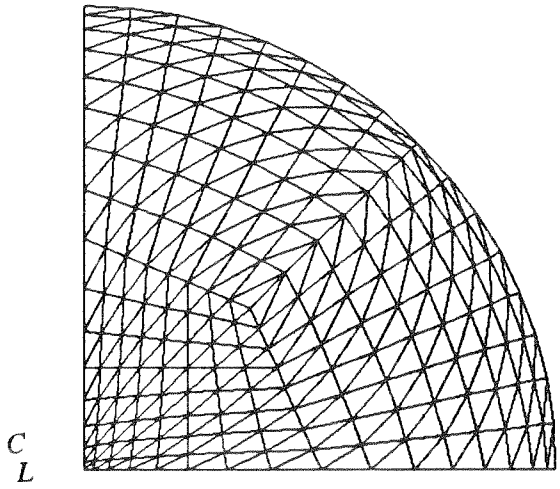

C
L

MC3

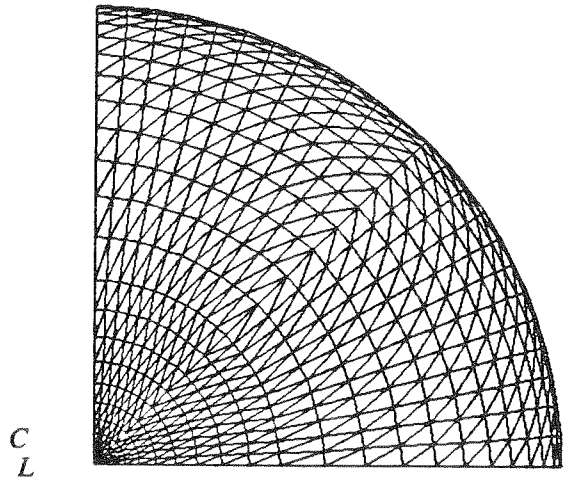

C
L

MC4

Fig. 4.4 Circular meshes

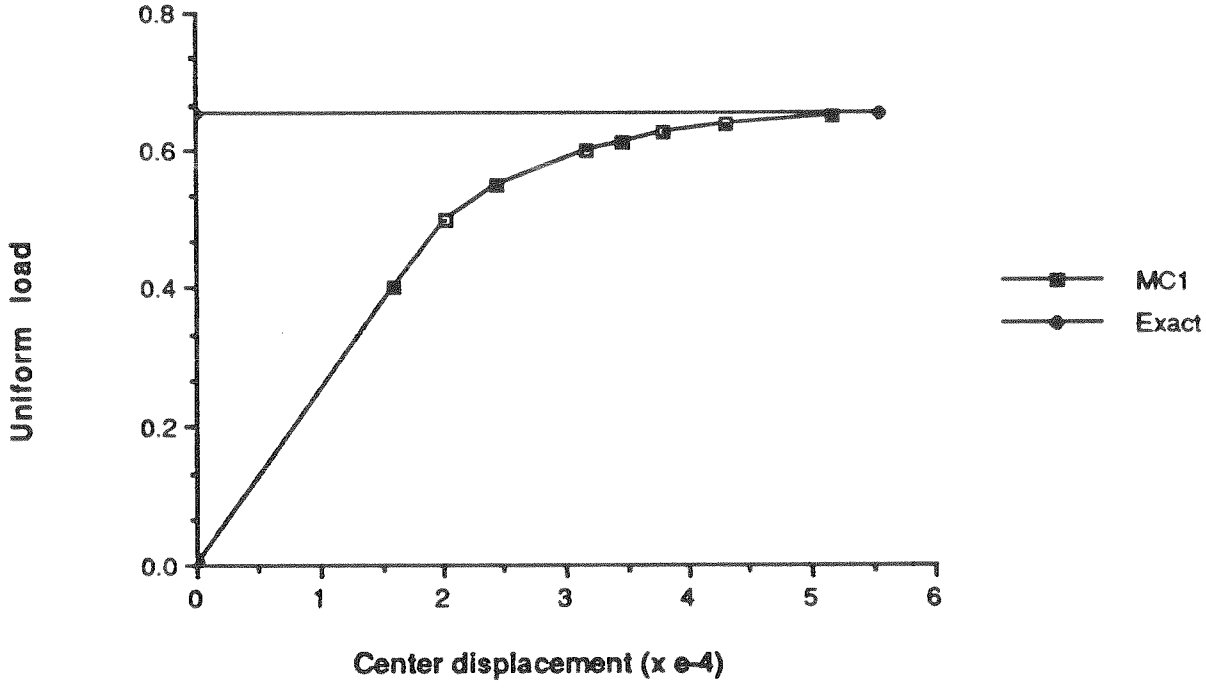

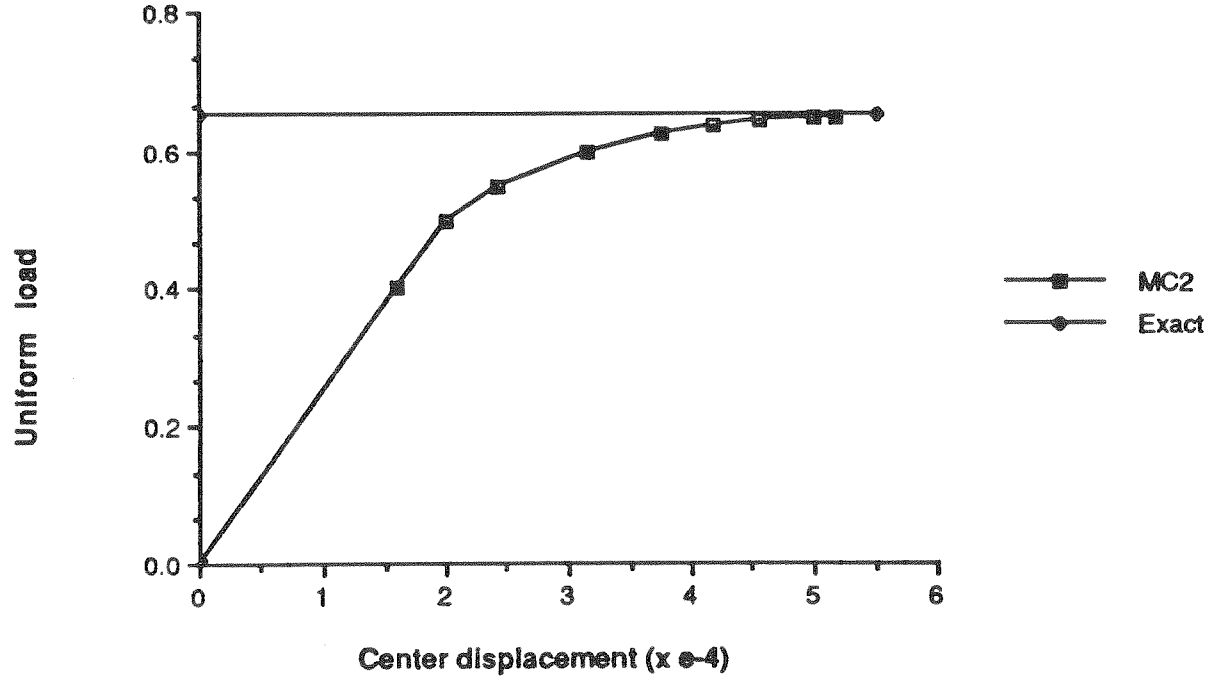

Fig. 4.4.1 Simply-supported uniformly loaded circular plate; load-displacement diagrams

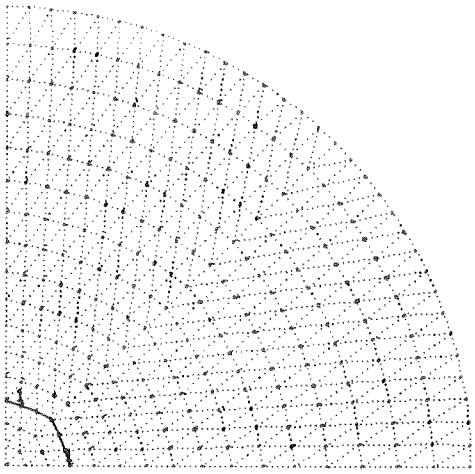

q=0.50

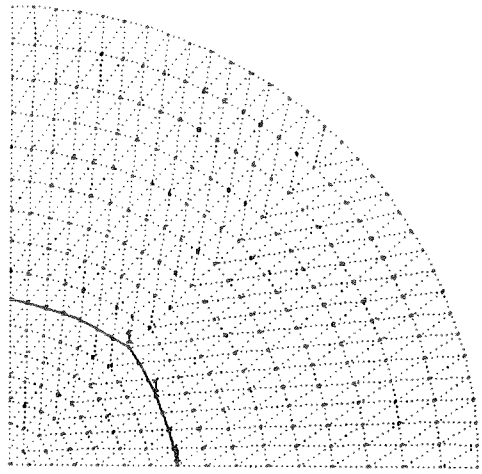

q=0.55

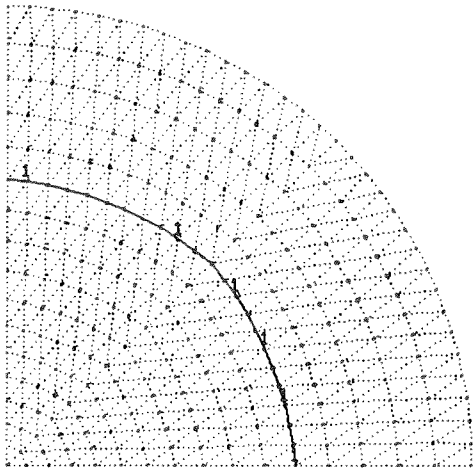

q=0.625

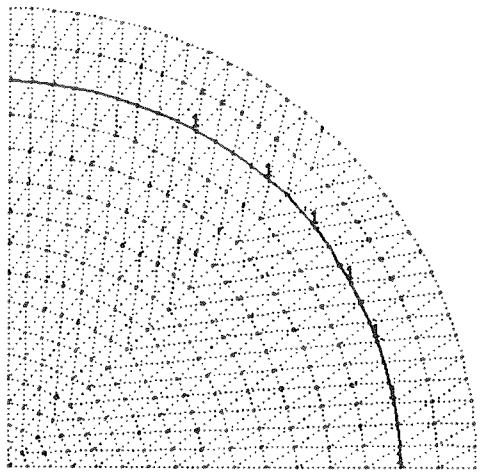

q=0.65

Fig. 4.4.2 Simply-supported uniformly loaded circular plate; evolution of plastic deformation (mesh MC2)

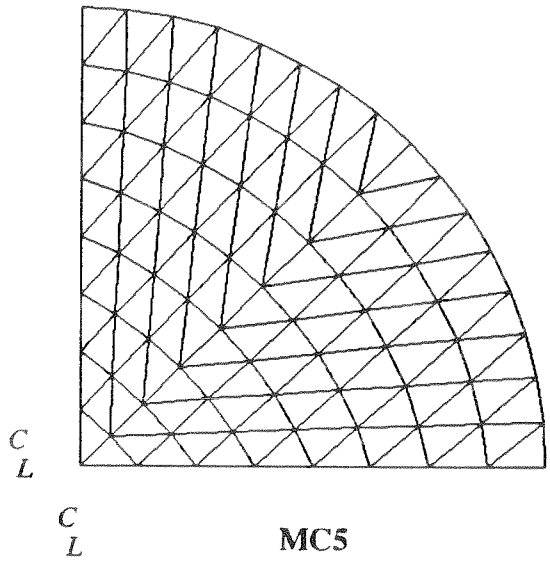

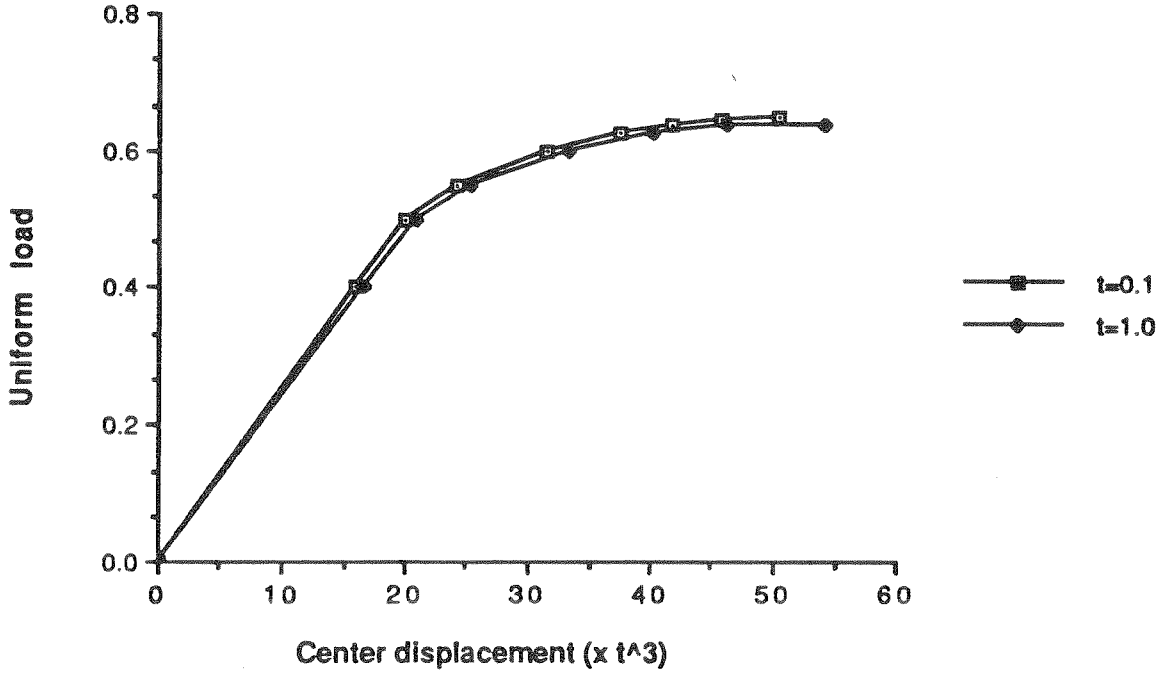

Fig. 4.4.3 Effect of transverse shear in plates with different thicknesses, but same ultimate moment

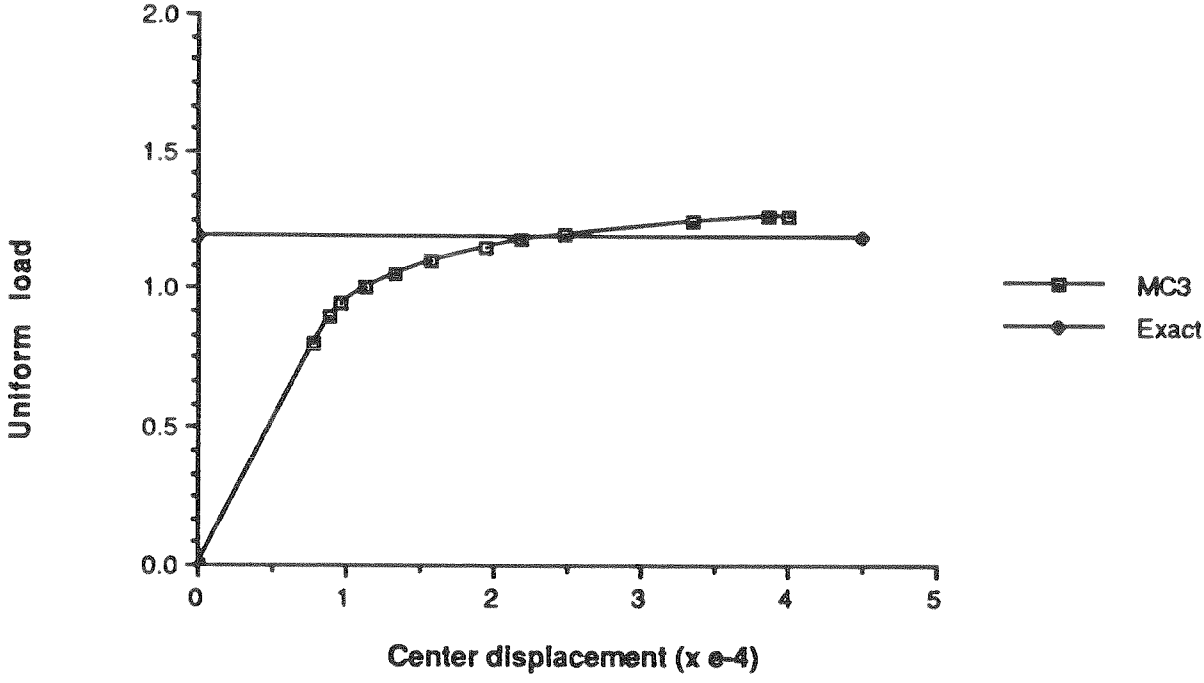

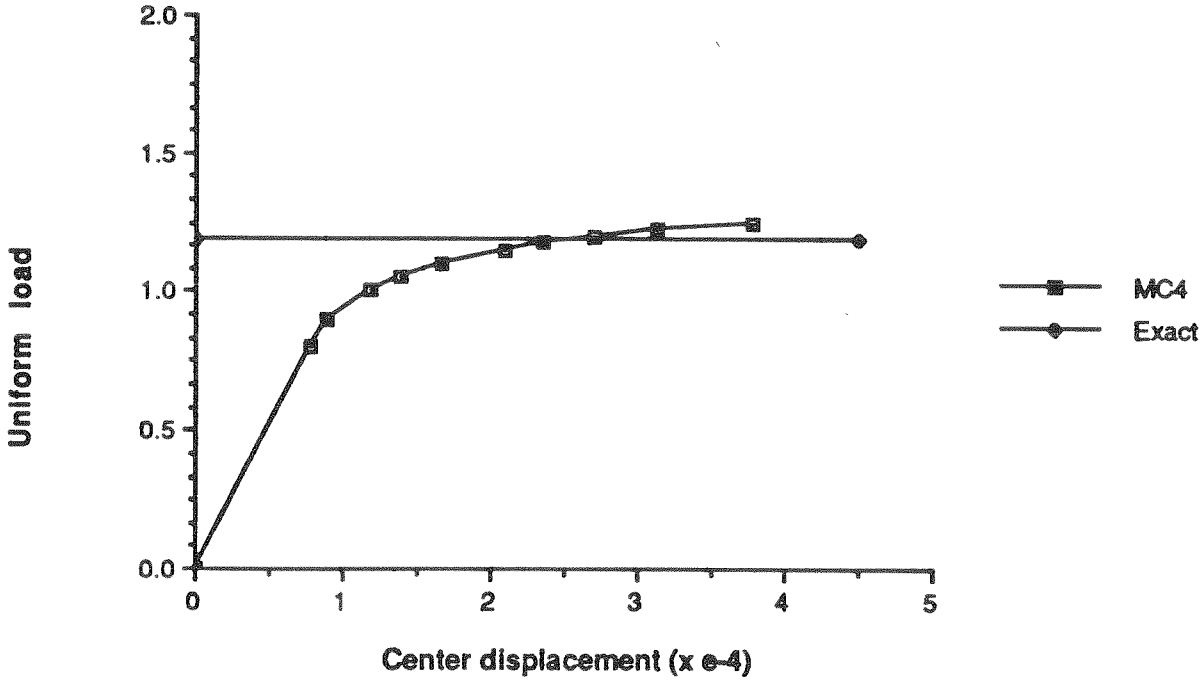

Fig. 4.5.1 Clamped uniformly loaded circular plate; load-displacement diagrams

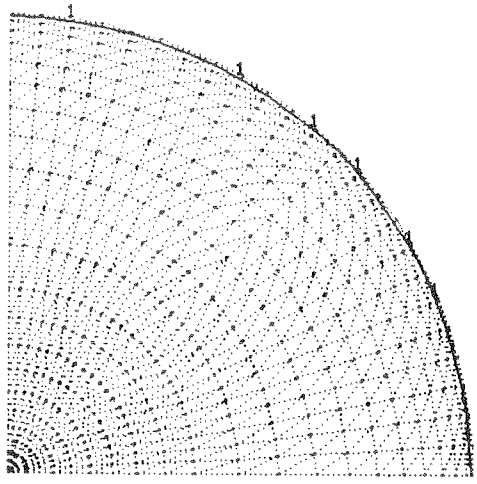

q=1.0

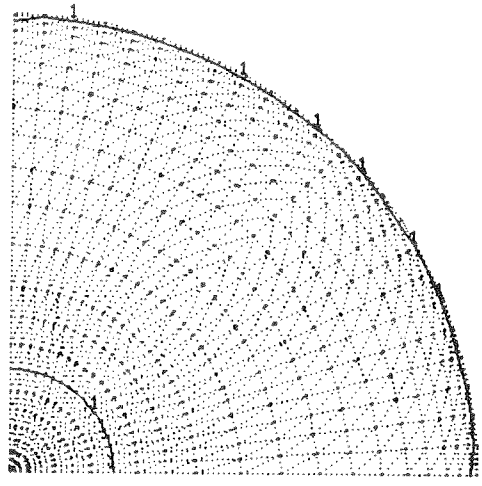

q=1.10

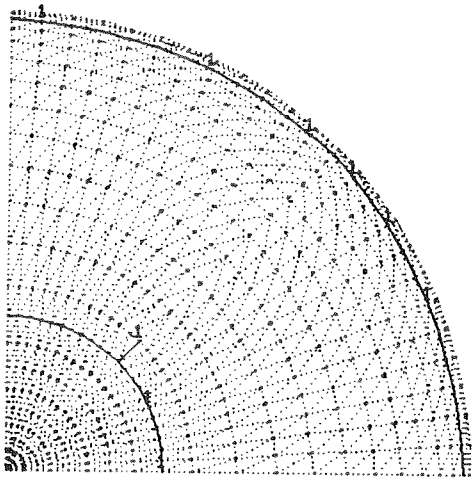

q=1.175

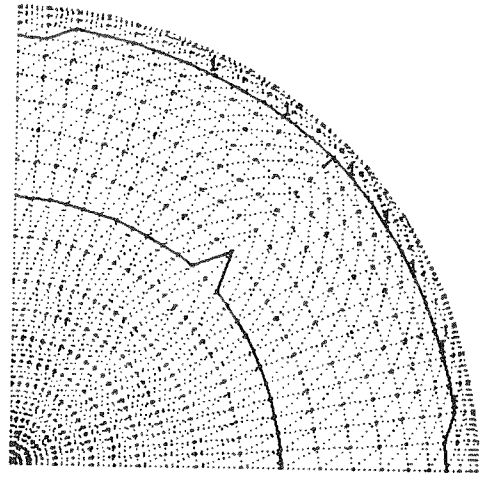

q=1.25

Fig. 4.5.2 Clamped uniformly loaded circular plate; evolution of plastic deformation (mesh MC4)

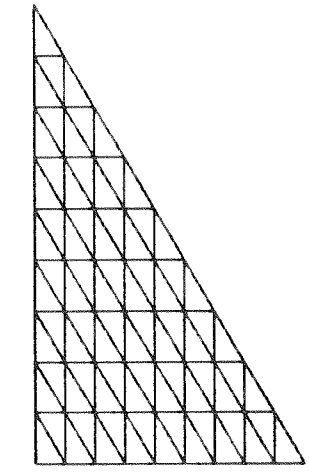

MT1

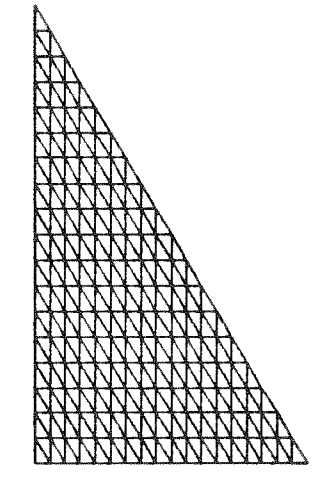

MT2

Fig. 4.6 Triangular meshes

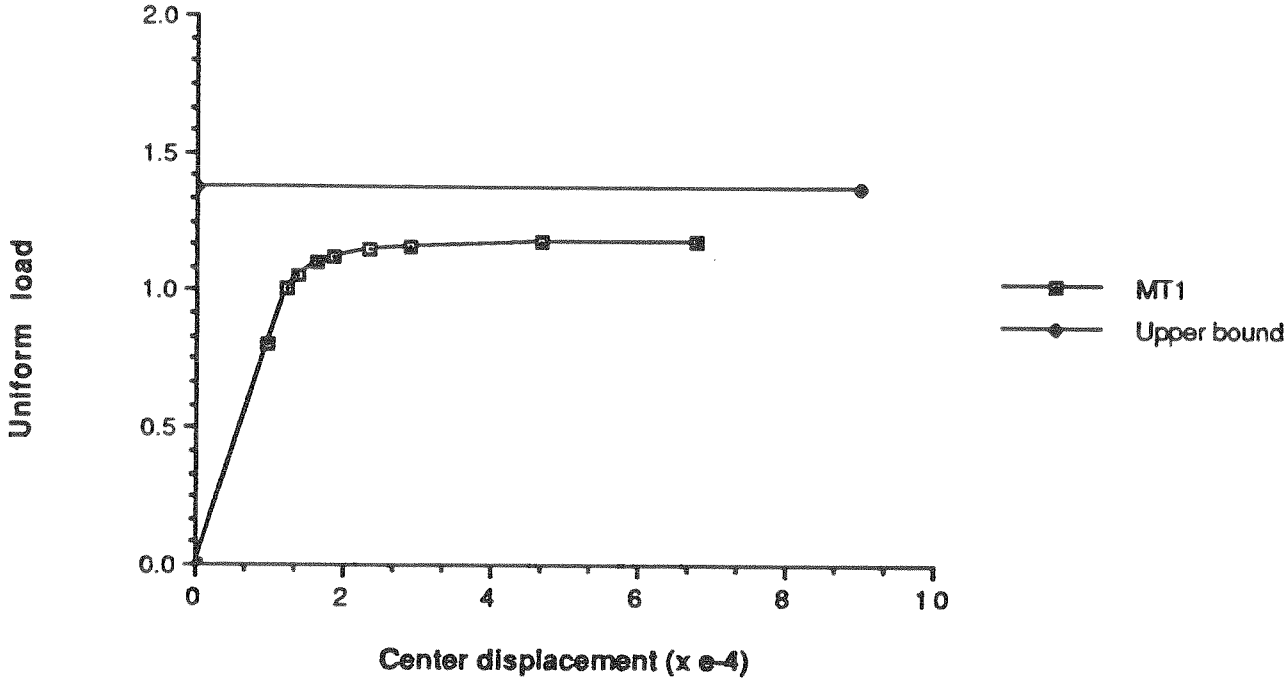

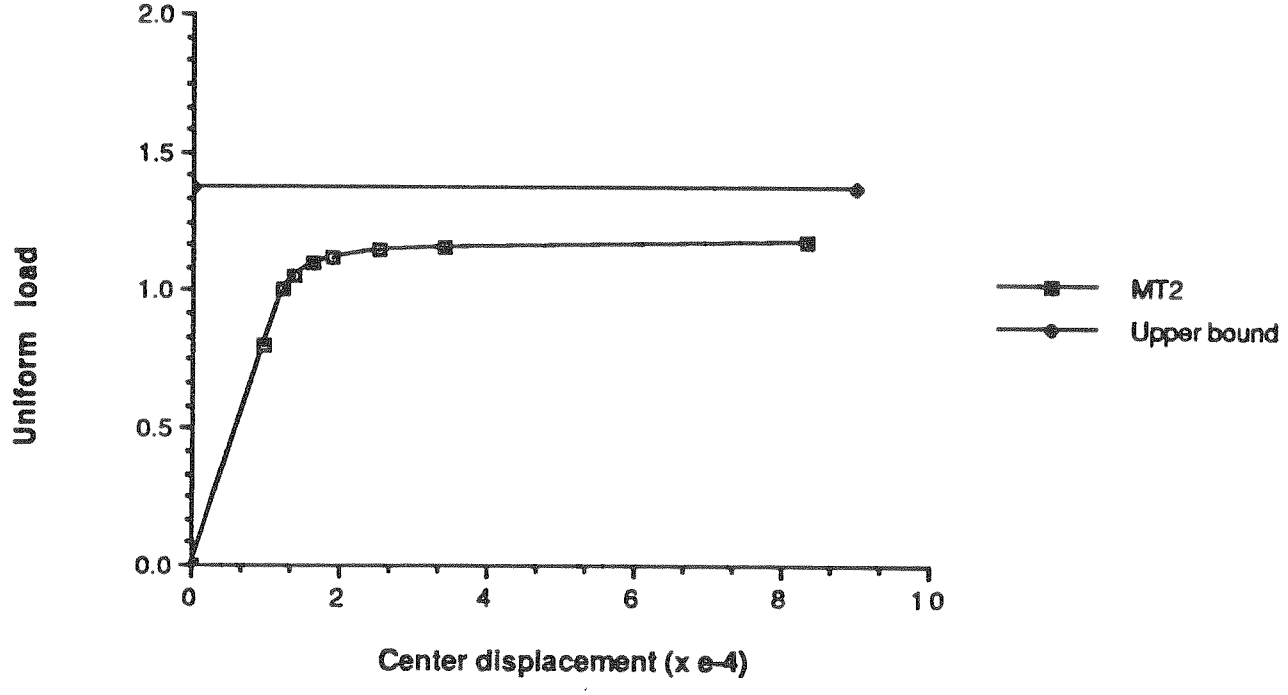

Fig. 4.6.1 Simply-supported uniformly loaded triangular plate; load-displacement diagrams

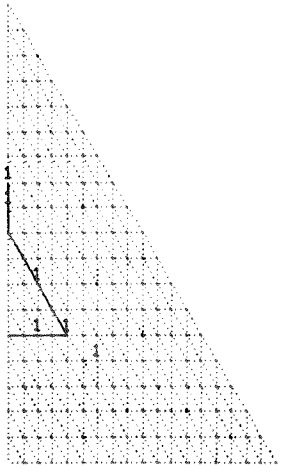

q=1.05

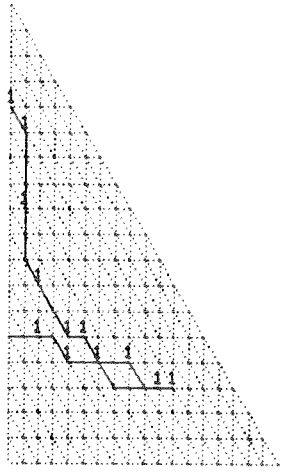

q=1.10

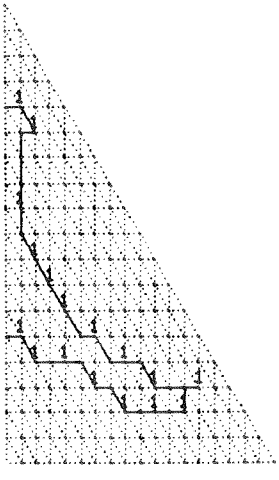

q=1.125

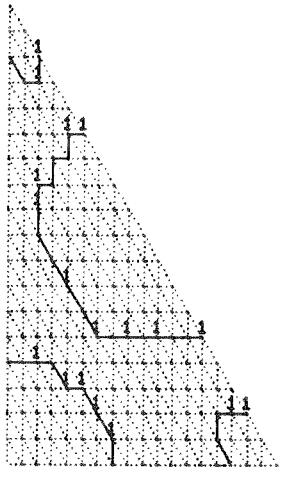

q=1.1625

Fig. 4.6.2 Simply-supported uniformly loaded triangular plate; evolution of plastic deformation (mesh MT2)